Electro-thermal computational fluid dynamics analysis of a prismatic lithium-ion battery pack

Arun K. Raj[a*], Simone Parisi[a], Roberto Agromayor[a], Srivastav Shruti[b], Cheenicode Kabeer Fairoja[c] and Fredrik Haglind[a]

[a]Technical University of Denmark, 2800 Kongens Lyngby, Denmark
[b]Department of Cell Development, TRATON R&D
[c]Department of Cell Testing & Validation, TRATON R&D
[*] Corresponding author e-mail: arkra@dtu.dk

Abstract:

Large-format prismatic lithium-ion batteries are increasingly used in electric buses, trucks, and other heavy-duty platforms where high energy density and compact packing are essential. Studying their thermal behaviour is critical because temperature governs safety margins, power capability, aging rates, and the risk of thermal runaway. In this study, we use a commercial computational software with electro-thermal coupling to conduct a transient, three-dimensional computational fluid dynamics investigation of a prismatic lithium-ion battery pack. The electro-thermal framework comprises anisotropic heat conduction in the cell, laminar-flow, conjugate heat transfer equations for the coolant, and a physics-based heat generation model. This study investigates the thermal performance of 2×4 large-format prismatic lithium-ion battery pack utilizing a Z-type cooling configuration. The main goal is to evaluate the temperature uniformity and heat dissipation efficiency by analysing the complex interplay between coolant flow rates (0.25 m/s to 1.5 m/s) and inter-cell spacing (3 mm to 10 mm) to optimize battery safety and longevity. The numerical model was validated using the experimental data from a commercial prismatic lithium-ion cell undergoing constant current-constant voltage cycling. The validation results show excellent agreement with the experimental temperature measurements with a maximum temperature difference of 0.25 K, demonstrating the predictive capability of the numerical model. The analysis indicates that, under a 1C rate discharge-charge cycle, the average cell temperature is more sensitive to variations in the coolant flow velocity than the inter-cell spacing. At a coolant flow rate of 1.5 m/s, the average cell temperature differs by 3 K compared to 0.25 m/s at an inter-cell spacing of 5 mm. Across the scenarios studied, a coolant velocity of 1.5 m/s with 5 mm inter-cell spacing is the best-case scenario for effective thermal dissipation.

Keywords:

Air-cooled; CC-CV cycle; Channel spacing; Large-format cells; Temperature gradients.

1. Introduction

The global transition toward electrified transportation is essential for reducing the greenhouse gas emissions and environmental impact of the road transport sector [1]. Electric vehicle adoption has accelerated rapidly in the passenger car market, but heavy-duty vehicles, and long-haul trucks in particular, lag significantly in electrification rates [2]. While battery mass is a secondary consideration in passenger vehicles, it is a critical constraint for heavy-duty trucks, where every kilogram added to the kerb weight directly reduces the profitable cargo the vehicle can carry. Consequently, the development of lightweight, cost-effective battery packs is therefore critical to the widespread adoption of zero-emission heavy-duty vehicles [3].

Battery packs for heavy-duty applications require significantly higher energy capacity than those for light-duty vehicles, making their longevity and reliability critical to the overall system cost. The lifetime of state-of-the-art lithium-ion battery packs is typically shorter than the service life of a truck, which underscores the importance of high-performance thermal management to maximize battery life and ensure economic viability [4]. Since battery degradation is strongly coupled to operating temperature, maintaining cells within the optimal range of 15 °C to 35 °C is essential to prevent accelerated capacity fade and extend operational life [5]. Temperatures exceeding 40 °C promote the growth of the solid electrolyte interphase (SEI) layer and increase internal electrical resistance, leading to capacity loss [6]. Furthermore, temperature non-uniformity across a pack may lead to electrical imbalances and localized deterioration, which can cause the premature failure of the battery pack [7].

Designing an effective Battery Thermal Management System (BTMS) requires balancing cooling performance against system mass, volume, and cost [5]. High-performance architectures typically rely on liquid cooling,

which offer high heat transfer coefficients and temperature uniformity. However, these systems require heavy auxiliary components, including pumps, coolant lines, and flow manifolds, while also introducing risks related to coolant leakage and high-voltage safety [7]. For heavy-duty trucks where weight and cost are critical constraints, air-based cooling is a compelling alternative due to its simplicity, lower manufacturing cost, and significantly lower system mass [8]. Air cooling, however, is characterized by lower convective heat transfer coefficients than liquid cooling, typically in the range of 10 W/m²·K to 100 W/m²·K [9]. The central research question for heavy-duty applications is therefore whether an optimized air-cooled architecture can provide adequate thermal control for large-format cells, ensuring safe operation and sufficient battery lifespan.

The current literature on the thermal management of lithium-ion batteries remains heavily focused on cylindrical cells, as they were the first to reach commercial maturity at a small scale [5,7]. However, the cylindrical geometry constrains the achievable capacity per cell, so meeting the energy requirements of heavy-duty applications with this format results in high cell counts and complex assembly processes. Prismatic cells, on the other hand, offer a stronger economic case for heavy-duty applications, providing higher packing efficiency, simpler module assembly, and higher volumetric energy density in space-constrained industrial packs [10]. Furthermore, the flat large-format faces of prismatic cells facilitate the design of uniform cooling channels and promote more consistent heat dissipation, which is advantageous for air-cooled systems [11].

Despite these advantages, existing studies on thermal management of prismatic packs predominantly focus on small-format cells that are not representative of the requirements of heavy-duty trucks [12-14]. This scale gap is critical because heat generation in a battery pack scale with its volume (L^3), while heat dissipation is limited by its surface area (L^2). Consequently, as cell capacity increases the difficulty to dissipate heat increases, and the findings from studies on 15 Ah [12] or 60 Ah [13] prismatic cells cannot be directly extrapolated to the 150+ Ah cells required for industrial heavy-duty applications.

Afzal *et al.* [15] conducted a steady-state, finite volume method-based laminar-flow analysis on prismatic battery cells to study the impact of cell spacing on heat generation and Reynolds number (Re). The study identified that narrow cell spacing leads to a decrease in cooling performance and better temperature uniformity can be achieved only by balancing Re, heat generation, and cell spacing. Argade and De [12] conducted a steady-state analysis on a Z-type cooling configuration of a prismatic battery pack using an open-source software – OpenFOAM. The findings suggested that increasing the air velocity from 3 m/s to 4.5 m/s reduced the maximum cell temperature by 4.6 K. Furthermore, the investigation showed that addition of secondary outlet on the top surface of the pack, can lower the maximum cell temperature by 1 K. Similarly, Zhang *et al.* [14] carried out a comparative study, including U-type and Z-type configurations to understand the effect of inlet and outlet positions on the airflow distribution inside a cylindrical lithium-ion battery pack. The findings indicated that the cooling efficiency still depends strongly on the air velocity. A comparison between U-type and Z-type cooling configurations showed that, at low air velocities, the U-type configuration exhibited poorer temperature uniformity than the Z-type configuration. However, as the air velocity increased, the Z-type configuration exhibits poorer temperature uniformity. This behaviour, however, depended on the chosen pack geometry and cell type [14].

Therefore, to develop an effective air-cooled BTMS for heavy-duty trucks, there is a need for transient, multi-physics models that resolve these coupled electrochemical and thermal-fluid interactions. For example. Investigating thermal management of high-capacity (150+ Ah) cells, presents a unique heat dissipation challenge due to their reduced surface-area-to-volume ratios compared to a low-capacity cells [12,13]. Unlike steady-state analysis [12,15], this work employs a transient analysis to capture the dynamic thermal response profiles essential for real-world operational safety. The present study employs a three-dimensional multi-physics model of a 2×4 large-format prismatic lithium-ion battery pack representative of heavy-duty vehicles. The model combines lumped battery electrochemistry, conjugate heat transfer, and fluid flow, enabling accurate predictions of the local temperature distribution within the pack. The numerical model is first validated against experimental data from a commercial 157 Ah Nickel Manganese Cobalt (NMC) prismatic cell subjected to constant current-constant voltage cycling at a 1C rate. The objectives of this work are threefold: (i) to quantify the effects of inter-cell spacing (3 mm to 10 mm) and coolant velocity (0 m/s to 1.5 m/s) on the average and maximum cell temperatures, (ii) to characterize the thermal disparity between the upstream and downstream sections of the pack, and (iii) to identify the inter-cell spacing and coolant flow velocity that best balance heat dissipation and pressure drop while minimizing temperature non-uniformity during 1C cycles.

The remainder of this paper is organized as follows: Section 2 details the computational framework. Section 3 presents and discusses the numerical results, focusing on the effect of inter-cell spacing and coolant velocity. Lastly, Section 4 concludes the study by highlighting the key findings of the work.

2. Computational framework and formulation

This section describes the computational framework used in this study, covering the geometry and mesh generation and the governing equations and physical models, as well as the boundary and initial conditions defining the problem. The section concludes with the solution strategy and convergence criteria.

2.1. Geometry and mesh

The battery pack consists of 8 cells arranged in 2 rows in parallel with 4 cells in series, as shown in Figure 1(a). A commercial prismatic Nickel Manganese Cobalt (NMC) lithium-ion cell with a rated capacity of 157 Ah and a nominal voltage of 3.2 V is considered in this study. The prismatic cell has dimensions 0.235 m (length) × 0.033 m (width) × 0.115 m (height). Each cell consists of an aluminium cathode tab and a copper anode tab. A Z-type parallel air-cooling configuration with an inlet and outlet width of 0.01 m and 0.014 m, and inlet and outlet length of 0.03 m and 0.1 m, respectively, is investigated. The Z-type configuration was selected primarily due to its ability to provide a more balanced airflow distribution across parallel cooling channels compared to the U-type configuration [16]. A 2-D schematic sketch with marked dimensions of the battery pack is shown in Figure 1(b). The inter-cell spacing (CS) in the pack is varied from 3 mm to 10 mm, depending on the case studied. The resulting inter-cell region is uniformly spaced and acts as the coolant passages. Air flowing through these passages is in direct contact with the cell surfaces, allowing heat generated within the cells to be dissipated away. Thermophysical properties of the materials used in the computational fluid dynamics (CFD) model are detailed in Table 1.

COMSOL Multiphysics v.6.3® was used to define the computational geometry and to generate the mesh. A user-controlled mesh was employed to discretize the computational domain. A hybrid hexahedral-tetrahedral element strategy characterized by a maximum skewness of 0.91 and an average skewness of 0.72 was adopted to capture the thermal and flow gradients. Figure 2 shows the computational mesh used for the present analysis.

Figure 3 depicts the sensitivity analysis of air outlet temperature across various mesh densities. Grid independence of the numerical results was verified through a systematic grid-refinement study. The

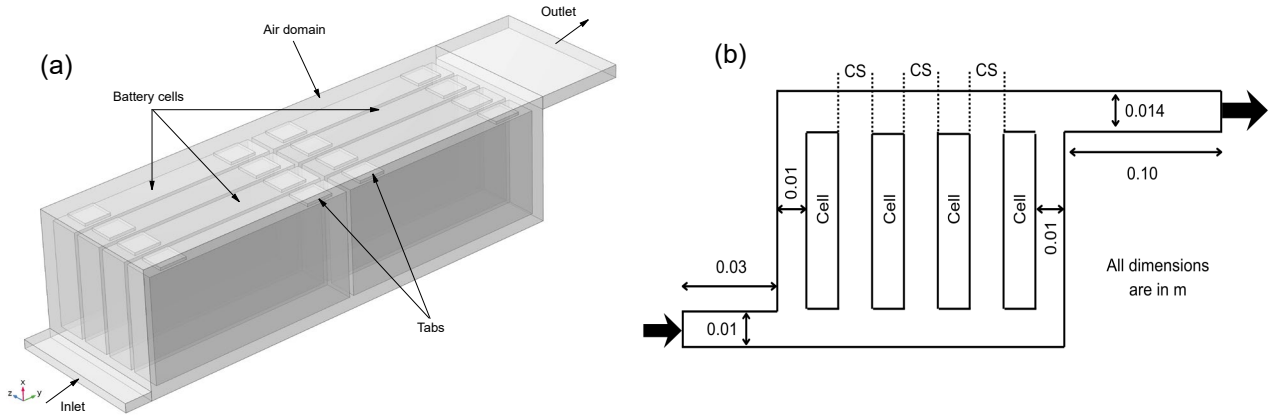

Figure. 1. *(a) Computational domain of battery pack, and (b) 2-D schematic sketch of the battery pack.*

Table 1. *Thermophysical properties of materials used in the model.*

Property	Cell (lithium-ion)	Aluminum	Cooper	Air (301.95 K)
Density (kg m^{-3})	2415	2700	8960	1.171
Specific heat (J kg^{-1} K^{-1})	941	900	385	1005.1
Dynamic viscosity (kg m^{-1} s^{-1})	–	–	–	1.85×10^{-5}
Thermal conductivity (W m^{-1} K^{-1})	1 (cross-plane), 30 (in-plane)	238	400	0.0264

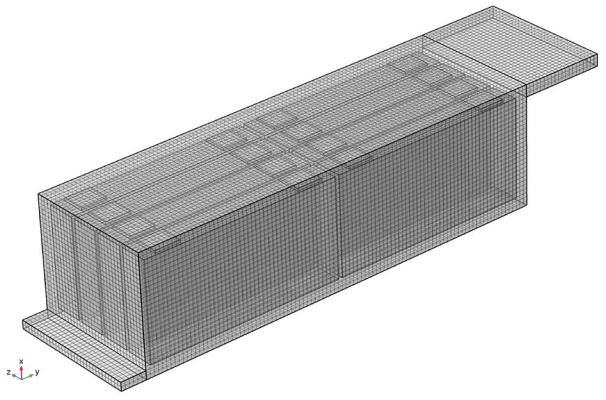

Figure. 2. *Discretized mesh of the battery pack computational domain.*

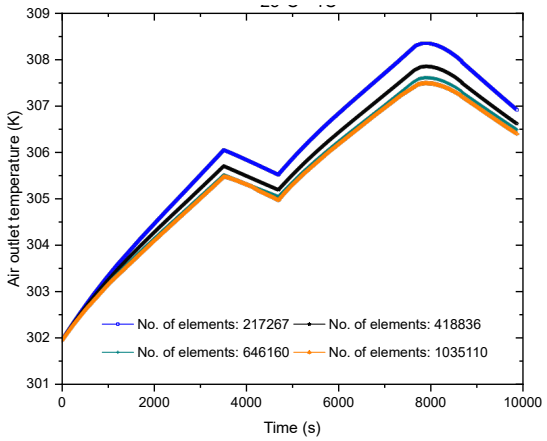

Figure. 3. *Grid independence test for the battery pack with CS = 5 mm and coolant velocity, u = 1.5 m/s.*

computational domain was discretized using four different mesh densities (i.e., 217,267, 418836, 646160, and 1,035,110), with refinement ratios ranging, from approximately 1.5 to 1.9. A key output parameter, namely air outlet temperature, was monitored for each mesh under a fixed battery pack configuration with an inter-cell spacing of 5 mm and a coolant velocity of 1.5 m/s. The observations indicate that the variation in the temperature became negligible, i.e., less than 0.08 % between the meshes containing 418,836 and 646,160 elements. Despite the small deviation (0.16 %) observed between the 217,267 and 418,836 element meshes, a finer mesh was selected to ensure better element quality and solution robustness. Consequently, the 418,836 elements mesh was selected for all subsequent simulations to balance high computational accuracy with reasonable computational time.

2.2. Governing equations

We employ a commercial finite element method based CFD tool – COMSOL Multiphysics v. 6.3® to study the electro-thermal behaviour of a prismatic lithium-ion battery pack. A transient, three-dimensional model is developed, governed by a system of equations representing electrochemical dynamics, fluid flow, and heat transfer. The lumped battery interface calculates the electrical response and heat generation under galvanostatic load, which is then coupled to the heat transfer in solids and fluids and laminar flow interfaces to simulate the cooling performance. The following section details the governing equations for the lumped battery, laminar flow, and heat transfer in solids and fluids interfaces as implemented.

2.2.1. Lumped battery model

The cell thermal behaviour is investigated using a lumped thermal approach. The lumped battery interface calculates the electrical response and volumetric heat generation of the prismatic cells. Under galvanostatic operation, the battery current (I_{cell}) is a time-dependent input corresponding to the 1C experimental rate. This work focuses only on ohmic losses, where the cell voltage (E_{cell}) is determined by the open-circuit potential (E_{ocp}) and the internal resistance (η_{IR}):

$$E_{cell} = E_{ocp}(SOC, T) - \eta_{IR}(T) \quad (1)$$

where $I_{cell} = I_{1C} \times C_{rate}$ and SOC is the state of charge. The C_{rate} is the cell charging or discharging rate and I_{1C} is the current applied to the cell at 1C charge or discharge rate which is [17]:

$$I_{1C} = \frac{Q_{cell,0}}{3600} \quad (2)$$

Here $Q_{cell,0}$ is the cell capacity and the initial cell state-of-charge (SOC_0) is set to 1. The open-circuit potential at the reference temperature (E_{ocp}) and its temperature dependence ($\partial E_{ocp}/\partial T$) are specified as SOC-dependent inputs. The lumped ohmic voltage loss associated with the electrolyte and electrodes is given by:

$$\eta_{IR} = \eta_{IR,1C} \times \frac{I_{cell}}{I_{1C}} \quad (3)$$

where $\eta_{IR,1C}$ denotes the ohmic overpotential at 1C. An Arrhenius formulation is adopted to couple the lumped model with the thermal model. Therefore, the parameter $\eta_{IR,1C}$ is defined as a function of the cell temperature and is represented as [17]:

$$\eta_{IR,1C} = \eta_{IR,1C,ref} \times exp\left[\frac{E_a}{R}\left(\frac{1}{T} - \frac{1}{T_{ref}}\right)\right] \quad (4)$$

Here $\eta_{IR,1C,ref}$ is the reference 1C ohmic overpotential, E_a is the activation energy that controls the temperature sensitivity (E_a= 24 kJmol^{-1} [18]), T_{ref} is the reference temperature (298.15 K), and R is the universal gas constant (8.314 Jmol^{-1}K^{-1}).

As the battery cell undergoes charge-discharge cycling, heat is generated due to flow of internal current (I_{cell}). The heat generation comprises two main contributors [19]:

$$q = I_{cell}\left(E_{ocp} - E_{cell}\right) - I_{cell}T\left(\frac{\partial E_{ocp}}{\partial T}\right) \quad (5)$$

where the first term represents the ohmic losses, and the second term represents the reversible entropic heat associated with the entropy change of the electrochemical reactions inside the cell.

2.2.2. Laminar flow model

The laminar flow interface is used to compute the velocity ($\vec{V}$) and pressure (p) fields of the coolant. In this work, the coolant fluid, i.e., air is considered as incompressible and the Reynolds number (Re) is calculated based on the hydraulic diameter (D_h). Based on the mass flow rate considered for the analysis, the value of inlet velocity is within the laminar flow regime (i.e., Re between 250 to 1500). Therefore, the laminar flow model solves the incompressible Navier-Stokes equation, ensuring the conservation of mass and momentum [17]:

$$\rho \nabla \cdot \vec{V} = 0 \quad (6)$$

$$\rho\left(\frac{D\vec{V}}{Dt}\right) = -\nabla p + \mu \nabla^2 \vec{V} + \rho_0 \vec{g} \beta (T - T_{ref}) \quad (7)$$

Energy equation (fluid):

$$\rho C_p\left(\frac{\partial T}{\partial t}\right) + \rho C_p\left(\vec{V}.\nabla \mathrm{T}\right) = \nabla.(kT) \quad (8)$$

where the last term of the momentum equation uses the Boussinesq approximation to simplify the buoyancy forces due to the variation in fluid density with temperature. Here ρ is the fluid density and μ is the dynamic viscosity, ρ_0 is the reference density, $\vec{g}$ is the gravitational acceleration, and β is the isobaric coefficient of thermal expansion. The flow equations are coupled to the thermal model via the non-isothermal flow multiphysics node, ensuring that energy and momentum equations are solved simultaneously. This is critical for high discharge-charge rates (i.e., 1C or higher), as the heat generated by the battery cells alters the fluid's temperature, which in turn modifies the buoyancy force and the fluid's dynamic viscosity, thereby affecting the overall convective heat transfer efficiency of the battery pack.

2.2.3. Heat transfer in solids

The heat transfer in solid interface governs the temperature distribution (T) throughout the battery pack and the cooling channels. The energy balance equation for the solid domain is expressed as:

$$\rho C_p\left(\frac{\partial T}{\partial t}\right) = \nabla.(kT) + q \quad (9)$$

Here k is the thermal conductivity and C_p is the specific heat capacity. In solid battery domains, the velocity vector ($\vec{V}$) is zero. The heat source term (q) represents the total heat generated due to electrochemical reactions, incorporating both irreversible ohmic heating and reversible entropic heating. In the fluid domain, the $\rho C_p\left(\vec{V}.\nabla \mathrm{T}\right)$ term (in Eqn. (8)) accounts for the convective heat transport provided by the coolant. Due to the layered structure of the prismatic cell, thermal conductivity is defined as a diagonal tensor with anisotropic values in the in-plane and cross-plane directions. The lower cross-plane conductivity represents the additional thermal resistance introduced by the multiple material interfaces stacked along the cell length.

2.3. Boundary and initial conditions

The numerical model is initialized at a uniform ambient temperature (T_{amb}) of 301.95 K, and specific boundary conditions are applied to each physics interface to represent the operating environment and the battery pack constraints. At initial state, time ($t = 0$), the entire the pack and the coolant are assumed to be in thermal equilibrium with the environment. The initial conditions are defined by a uniform ambient temperature T_{amb}, and state-of-charge is SOC_0. Initially, the fluid velocity ($\vec{V}$) and pressure (p) are equal to zero. The electrical behaviour of the cells is governed by the galvanostatic load and the current (I_{cell}) is a time-dependent input based on the experimental data for 1C rate. For buoyancy-driven cases, the gravitational acceleration is plugged in conjunction with the Boussinesq approximation. Under natural convection, the inlet and outlet face of the pack are treated as closed boundaries while the side faces of the battery pack facilitate heat exchange with the surroundings. For the forced convection, the flow is assumed to be fully developed, and an average velocity of u_{avg} is applied at the inlet face of the pack. This work covers a velocity range corresponding to Re values between 250 and 1500. An outflow pressure boundary condition is applied at the outlet face of the pack, where the pressure is set to $p = 1$ atm to represent discharge to ambient conditions. For the forced convection scenario, the coolant enters the pack at T_{amb}. A no-slip condition is applied to all the solid surfaces in contact with the fluid. The exterior surfaces of the battery pack (apart from the inlet and outlet) are treated as adiabatic surfaces. At the interface between the prismatic cells and the coolant, a conjugate heat transfer condition is applied. This condition requires both temperature and heat flux to be continuous across the interface. The balance of normal heat fluxes is expressed as:

$$k_{cell}\left(\frac{\partial T_{cell}}{\partial \hat{n}}\right) = k_{air}\left(\frac{\partial T_{air}}{\partial \hat{n}}\right) \quad (10)$$

Here k_{cell} is the anisotropic thermal conductivity tensor and k_{air} is the air's scalar thermal conductivity. At this interface, a no-slip boundary condition is imposed for the fluid flow. In natural convection cases, buoyancy effects are accounted for in the fluid momentum equations through the Boussinesq approximation.

2.4. Solution procedure and convergence criteria

The coupled electro-thermal model was solved using a multi-step approach to ensure numerical stability and computational efficiency. By default, the laminar flow interface employed finite element method formulations. For the forced convection cases, the solution procedure consisted of two steps: (a) Step 1 (stationary): A stationary simulation was first executed to solve for the steady-state velocity and pressure fields of the cooling fluid. In this step, the battery heat source was inactive, and the fluid properties were evaluated at the initial ambient temperature. This provided a fully developed laminar flow profile as a robust initial condition for the subsequent step. (b) Step 2 (time-dependent): Using the solution from Step 1 as the initial values, a transient simulation was performed to simulate the 1C discharge-charge cycle. During this stage, the lumped battery interface calculated the time-varying heat source, and the heat transfer interface solved for the evolving temperature field, which was fully coupled to the fluid domain. The transient behaviour was resolved using the backward differentiation formula for time integration. This method was chosen for its stability in handling the stiff non-linearities inherent in battery thermal responses. Automatic time stepping was employed to maintain

a balance between temporal resolution and calculation time. For the velocity and pressure fields, the simulation utilizes P1+P1 discretization, where both the velocity components and the pressure were represented by linear shape functions (first-order Lagrange elements). The temperature field was also discretized using linear Lagrange elements. The variables associated with the lumped battery interface were governed by global equations that do not require spatial discretization but were solved as a system of differential algebraic equations across the battery domains.

To ensure the numerical convergence of the transient electro-thermal simulation, the solution at each time step was considered converged when the relative tolerance for the dependent variables (velocity, pressure, temperature) satisfies a strict threshold (relative tolerance, $Res_{tol} \leq 10^{-4}$). To monitor the stability of the solution in real-time, several domain and boundary probes were strategically placed within the battery pack. These probes track average cell temperature, maximum cell temperature, air outlet temperature, and voltage. Convergence was further verified by ensuring that the temporal evolution of these probes was smooth and free of unphysical oscillations. For all cases studied, a mass balance check in the fluid domain was performed to ensure that the difference between mass flow rate at the inlet and outlet is negligible.

3. Results and discussion

This section discusses the numerical results and is divided into three parts: Section 3.1. details the model fitting and validation step, Section 3.2. discusses the effect of inter-cell spacing, and Section 3.3. describes the effect of coolant velocity. The focus is on identifying the average cell temperature obtained corresponding to the different sets of numerical simulation carried out under a 1C constant current-constant voltage (CC-CV) cycle. For all cases, the simulation time was set to 9920 s to match the duration of the experimentally measured 1C discharge-charge cycle. Specific focus is placed on how the temperature-dependent ohmic resistance, governed by the Arrhenius relationship, influences the total heat generation and the subsequent thermal management requirements in both natural and forced convection regimes.

3.1. Model fitting and validation

Parameter estimation was performed using least-squares minimization on a single-cell domain. Because the exact geometry of the test chamber was unavailable, natural convection was modelled using a convective heat transfer coefficient. A grid independence study was carried out, as shown in Fig. 4, revealing negligible deviations for all investigated meshes. The objective of the parameter fitting is to minimize the deviation between the measured and simulated signals for both temperature and voltage. The two deviation signals were added in a single objective function, with automatic scaling employed to ensure the two distinct quantities are comparable in magnitude.

The experimental data comprised a full discharge-charge cycle on a prismatic NMC-cathode cell, utilizing a constant-current constant-voltage protocol with a current of 1C, calculated from a nominal capacity of 157 Ah. The measurement tolerances, based on instrument specifications, are ±2.4 mV for voltage, ±150 mA for current, and ±1 °C for temperature.

A total of eight parameters were fitted: the actual cell capacity Q_{cell}, the second-order polynomial coefficients of the reference overpotential $\eta_{IR,1C,ref}\ (SOC)$, the first-order polynomial coefficients of the open-circuit voltage with respect to temperature $\frac{\partial E_{ocp}}{\partial T}\ (SOC)$, the specific heat capacity of the battery C_p, and the convective heat transfer coefficient h.

All variables were scaled to an order of magnitude of unity. The Levenberg-Marquardt algorithm, in conjunction with first-order accurate finite-difference gradient, was employed for the optimization. Initial parameter guesses were determined through preliminary manual fitting; consequently, the final optimization run reduced the objective function by a factor of two before converging. Post-optimization, the mean and standard deviation of

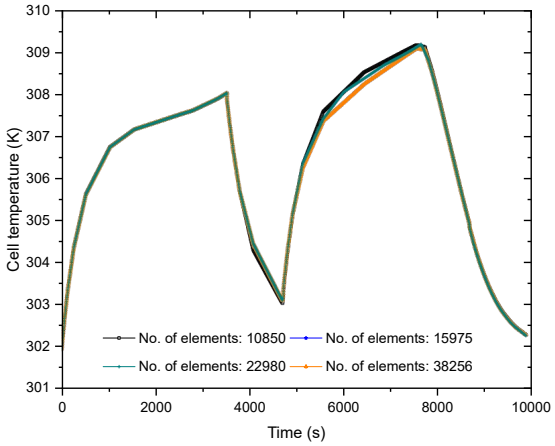

Figure. 4. *Grid-independence for the prismatic cell.*

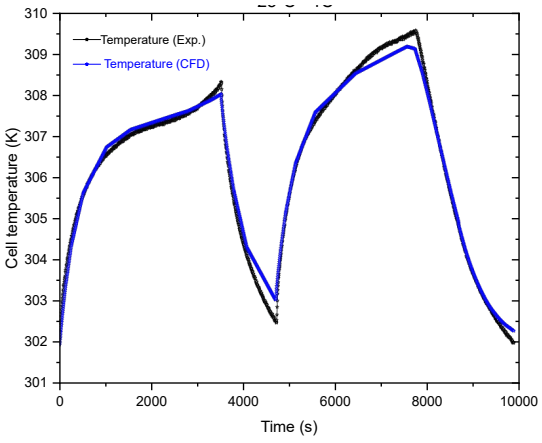

Figure. 5. *Validation curves of cell temperatures obtained from numerical and experimental data.*

the voltage deviation was 0.0025±0.03119 V, and 0.010±0.205 K for the temperature deviation. These quantitative metrics, combined with the qualitative agreement of all time-series features (as shown in Fig. 5), indicate a highly satisfactory model fit.

3.2. Effect of inter-cell spacing

In a prismatic battery pack, optimizing the inter-cell spacing is an important aspect for balancing volumetric energy density and thermal stability. In a Z-type cooling configuration, the inter-cell spacing arrangement of the 8 cells directly influences the internal hydraulic resistance and the resulting airflow distribution between the upstream and downstream cell sections of the pack. An inter-cell spacing lower bound of 3 mm and an upper bound of 10 mm was chosen to represent the critical design window for air-cooled pack. A cell spacing of less than 3 mm results in extremely narrow cooling channels, creating excessive hydraulic resistance and merged thermal boundary layers that hinder heat dissipation. Conversely, increasing the cell spacing more than 10 mm reduces the volumetric energy density and increases the overall structural footprint of the cell assembly. The selected inter-cell spacing range (3 mm to 10 mm) was consistent with the prior numerical study reported by Asif *et al.* [15]. Therefore, by analysing the spatial distribution range of 3 mm, 4 mm, 5 mm, 6 mm, and 10 mm, we aim to identify the suitable inter-cell spacing for the designed Z-type cooling configuration.

Figure 6 shows the comparison between average and maximum cell temperatures under forced and natural convection regimes. As evident from Fig. 6, for forced convection (inlet average velocity = 1.5 m/s), both average and maximum cell temperatures decrease with an increase in the cell spacing. At a fixed inlet average velocity, increasing the spacing leads to lowering the overall hydraulic resistance of coolant passages within the pack. This allows a larger volume of fresh, cool air to penetrate deeper into the pack rather than being restricted to the upstream section. Consequently, the downstream cells typically experience the maximum temperature due to the upstream pre-heated air encountering these cell surfaces.

Figure 7 depicts the average cell temperature contours for four different cell spacings (3 mm, 4 mm, 5 mm, and 10 mm), showcasing the temperature disparity between the upstream and downstream cells. The ability of the coolant to penetrate deeper into the pack with increase in cell spacing is also noticeable from these contour plots. Additionally, wider spacing allows to delay the merging of thermal boundary layers from adjacent cell surfaces, thereby maintaining a steeper local temperature gradient between the coolant and the cell surface. This promotes effective convective heat transfer coefficient and reduces the rate of coolant temperature rise along the flow direction The results suggest that the average cell temperature decreases from 307.91 K to 306.89 K corresponding to a cell spacing of 3 mm and 10 mm, respectively. Notably, the temperature difference of average cell temperature for cell spacing of 3 mm to 6 mm is less than 0.5 K, suggesting that an inter-cell spacing of 5 mm is a suitable choice for further investigation. In line with the earlier observations, the maximum cell temperature obtained for the cell spacings of 3 mm and 10 mm are 309.38 K and 308.50 K, respectively. Our findings for forced convection were consistent with the findings of Asif *et al.* [15], who reported that for a prismatic lithium-ion battery cell within a rectangular housing, the recommended inter-cell depended on the cell length and was below 10 mm for this case.

On the other hand, under natural convection (as shown in Fig. 6), the average and maximum cell temperatures increase slightly as the cell spacing increases from 3 mm to 10 mm. Despite the increase in the pack area (which increases the heat transfer surface), increasing the cell spacing introduces additional air in the pack,

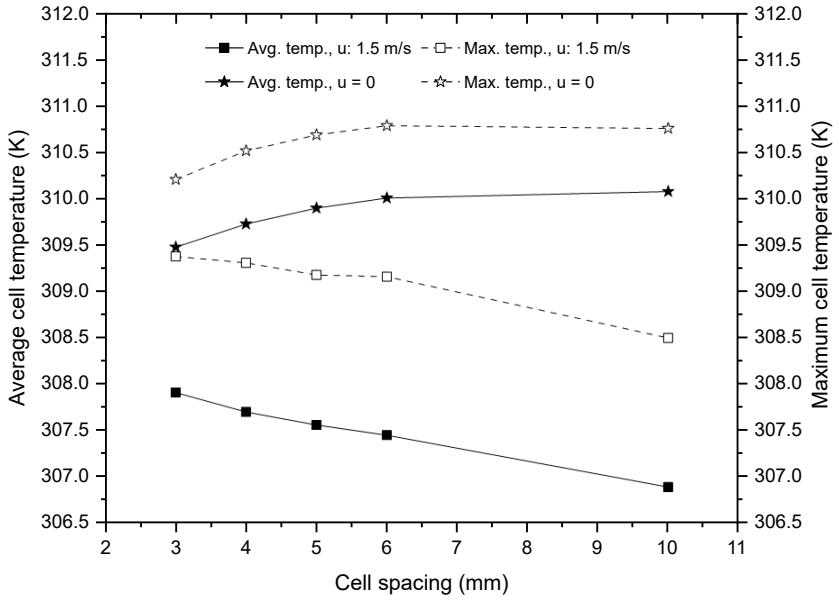

Figure. 6. *Comparison of average (left y-axis) and maximum (right y-axis) cell temperatures for forced convection (inlet velocity = 1.5 m/s) and natural convection (inlet velocity = 0).*

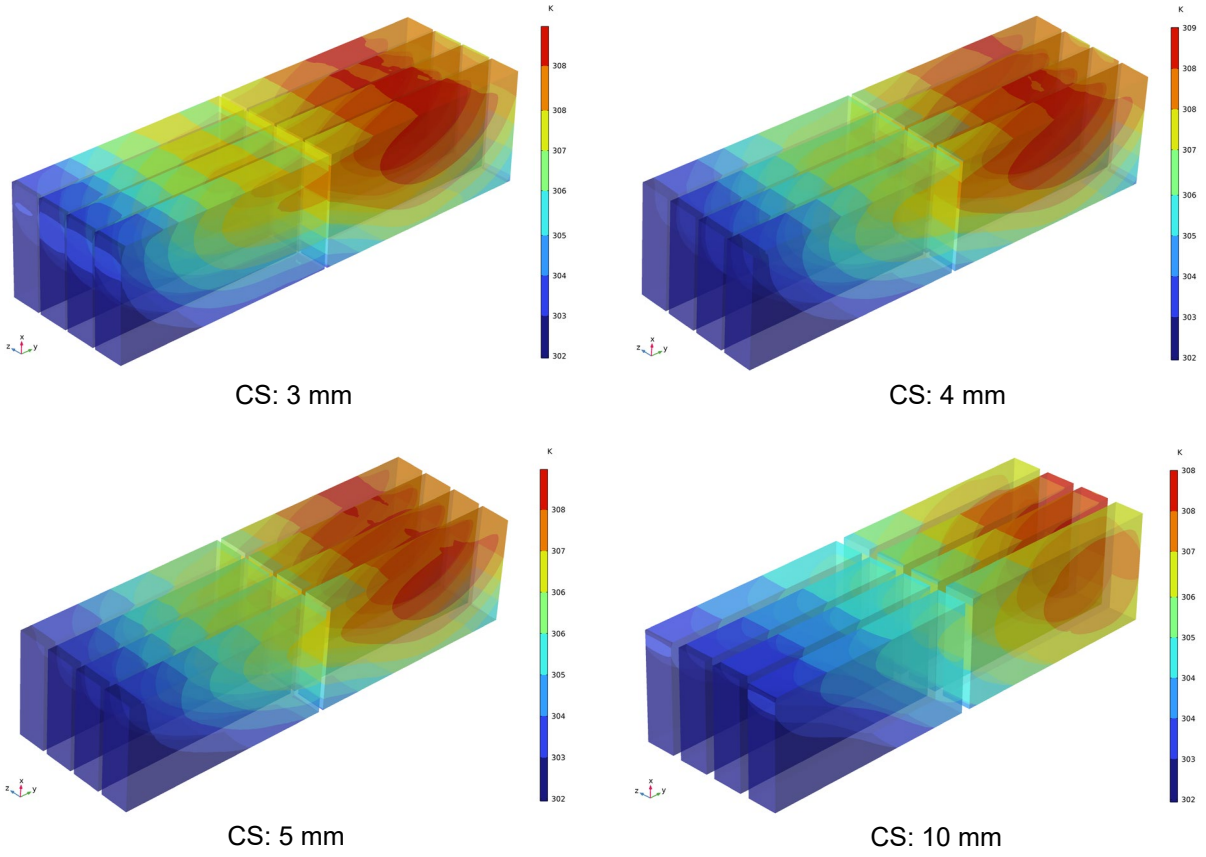

Figure. 7. *Spatial distribution of average cell temperature at four different inter-cell spacing (CS) under forced convection (inlet velocity = 1.5 m/s).*

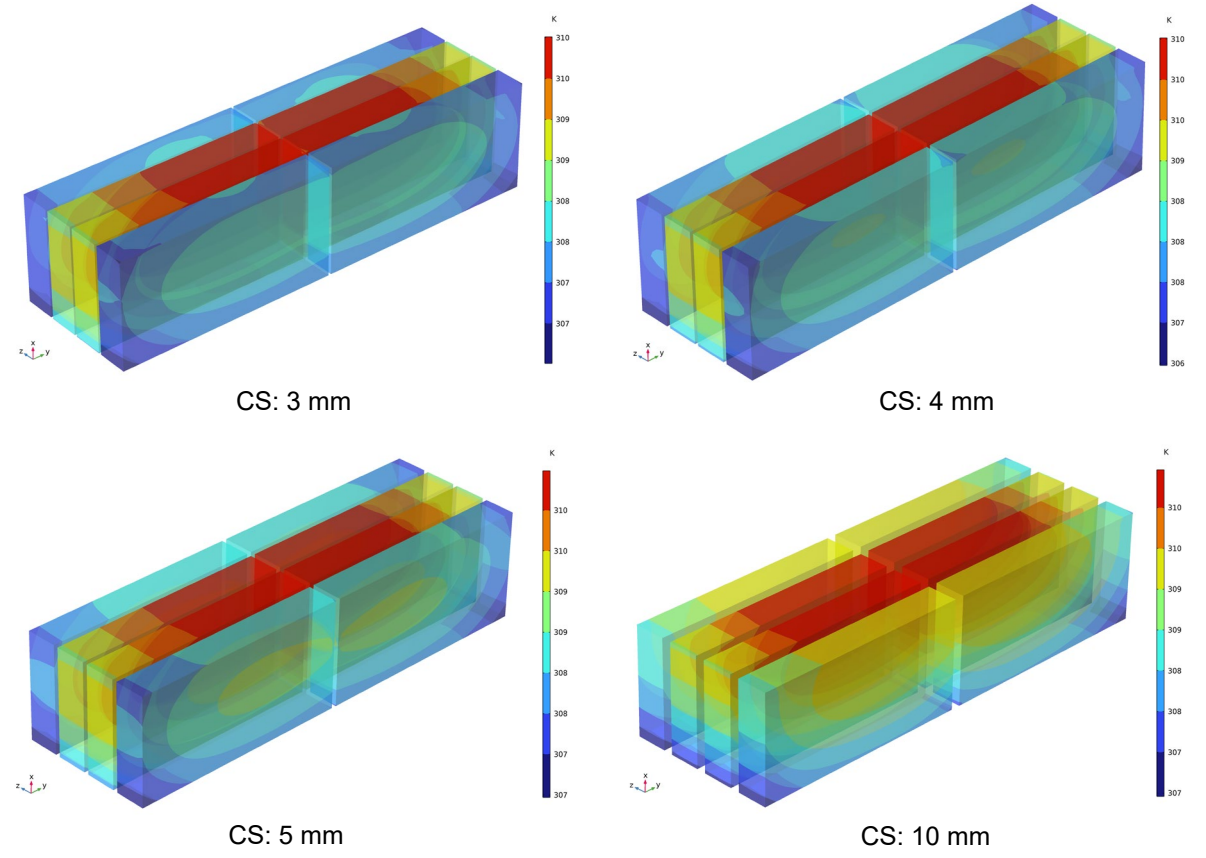

Figure. 8. *Spatial distribution of average cell temperature at four different inter-cell spacing (CS) under natural convection.*

acting as an insulator. This explanation is supported by the contours and its corresponding values of the average pack wall temperature, which decreases as the spacing increases. The average and maximum cell temperatures corresponding to a spacing of 3 mm are 309.48 K and 310.21 K, whereas for the spacing of 10 mm are 310.08 K and 310.76 K, respectively. These results identify the critical transition point where increasing the cell spacing, while beneficial for forced convection, becomes less attractive in closed environments due to stagnant air and thermal stratification. Therefore, for passive thermal management design, cell spacing must be carefully balanced to prevent the pack from becoming a heat trap. Figure 8 shows the average cell temperature contours under natural convection case across four different cell spacing. It is evident that the average cell temperature is comparatively lower at narrow spacing than wider spacing. Furthermore, these contours exhibit distinct heating pattern, where the central cells exhibit significantly higher temperatures than those at the periphery. This observed pattern is due to the thermal shielding effect, where inner cells lack direct access to the cooler boundary air and instead interact with air that has been pre-heated by adjacent cells.

3.3. Effect of coolant velocity

Thermal management of high-aspect-ratio surfaces of prismatic cells is greatly influenced by the convection heat transfer. This is, in turn, a direct function of the coolant velocity, which influences not only the heat dissipation and pressure drop but also the flow distribution uniformity across the parallel channels. Therefore, finding an optimal coolant velocity is essential to maintain the pack within the desired electrochemical heating window and to mitigate the thermal gradients that could affect the battery health and longevity. A Reynolds number range between 250 and 1500 was selected to understand the performance under laminar flow regime, which reflects the operating conditions for an energy-efficient, air-cooled battery modules, especially under standard 1C discharge-charge cycle for heavy-duty electric vehicles.

Figure 9 illustrates the effect of coolant velocity on the pack at an inter-cell spacing of 5 mm, considering different inlet average velocities of the coolant. As observed, there is a nonlinear decay of the average cell temperature from 310.84 K to 307.85 K as the velocity increases from 0.25 m/s to 1.5 m/s, respectively. The sensitivity of the average cell temperature to changes in inlet velocity is relatively higher in the low-velocity regime than in the high-velocity regime. The results indicate that the average cell temperature difference between coolant velocity of 0.25 m/s and 0.5 m/s is 0.86 K. Beyond a certain threshold, further increases in velocity yield smaller reductions in temperature because the system becomes limited by the conductive resistance within the cell itself rather than the convective resistance at the cell surface. This is evident from the results of average cell temperature at 1.25 m/s (308.06 K) and 1.5 m/s (307.85 K).

Figure 10 depicts the spatial distribution of average cell temperature across four different flow velocities. At lower velocities, a clear thermal gradient is visible, with higher temperatures localized toward the downstream cell section, where the air has already absorbed significant heat. As the velocity increases to 1.5 m/s, the cell at the upstream section shows a marked reduction in temperature and a comparatively lower temperature localization at the downstream section. These contours directly support the observations made in Fig. 9. The observed trend for prismatic cells was consistent with the results of Zhang *et al.* [14], who reported a similar decrease in average cell temperature with increasing coolant velocity in Z-type cooling configurations for cylindrical lithium-ion cells. Furthermore, the decreasing sensitivity of average cell temperature with increasing coolant velocity was reported also by Shi *et al.* [13] for prismatic lithium-ion batteries enclosed in a rectangular cooling domain. Overall, these comparisons show the influence of flow distribution and the inverse relationship between coolant velocity and average cell temperature, which is a fundamental performance characteristic of the pack.

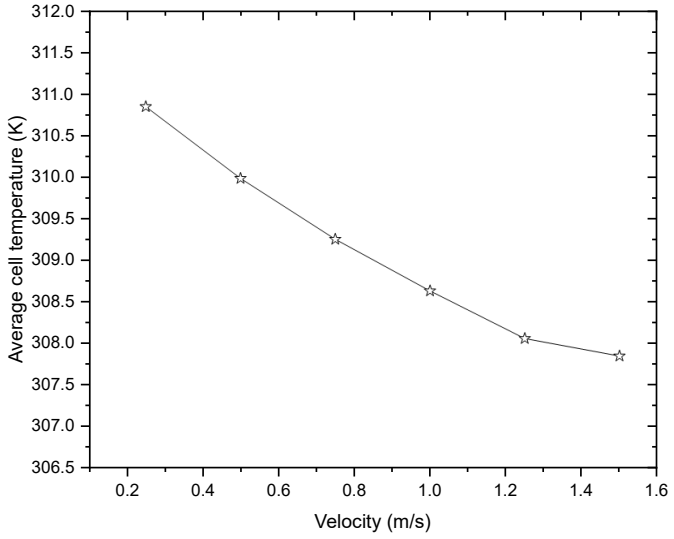

Figure. 9. *Average cell temperature as a function of coolant velocity at a fixed inter-cell spacing (CS) of 5 mm.*

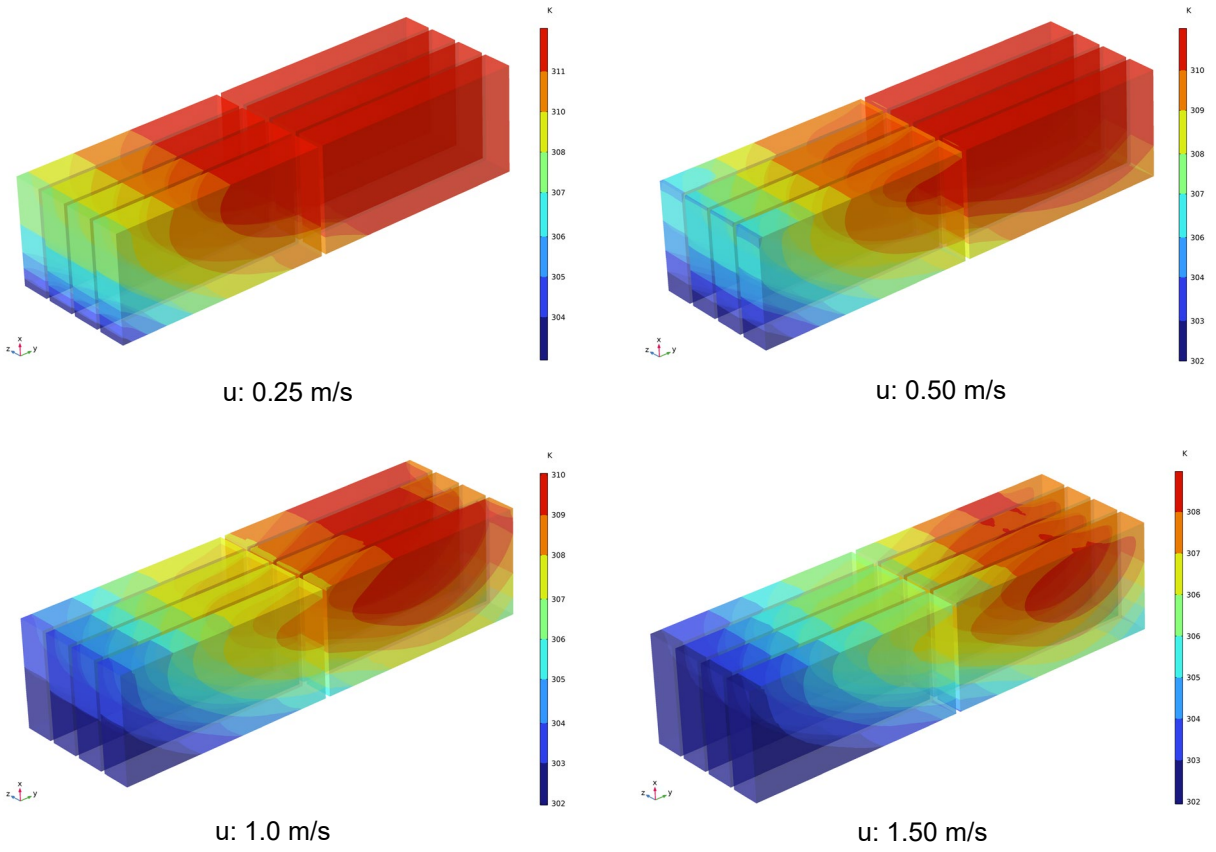

Figure. 10. *Spatial distribution of average cell temperature at four different coolant velocities corresponding to an inter-cell spacing (CS) of 5 mm.*

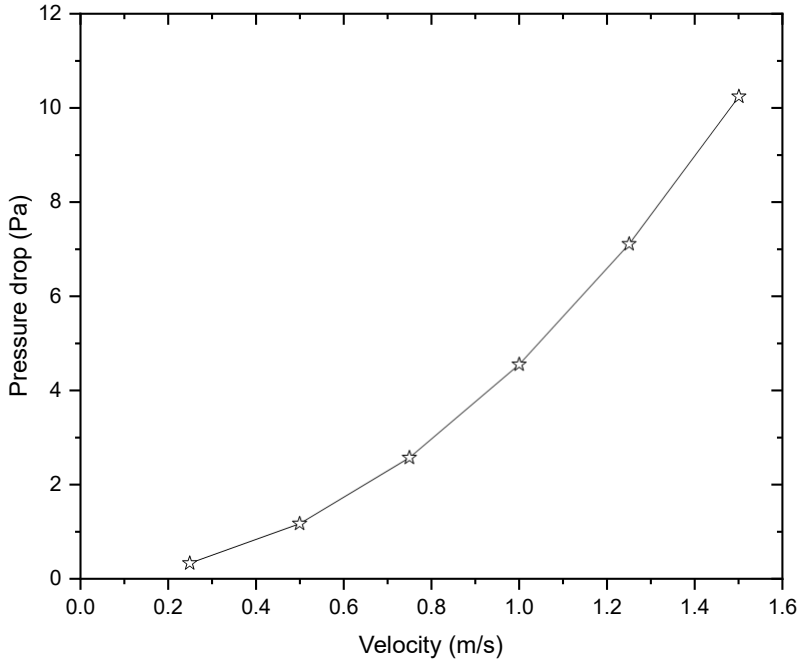

Figure. 11. *Variation of pressure drop across different coolant velocities corresponding to an inter-cell spacing (CS) of 5 mm.*

The hydraulic performance of the Z-type pack is also characterised by the pressure drop. Figure 11 shows the variation of pressure drop across different coolant velocities at a fixed inter-cell spacing of 5 mm. At the lowest velocity of 0.25 m/s, a negligible pressure drop of 0.34 Pa is obtained. However, as velocity increases to 1.5 m/s, the pressure drop increases to 10.23 Pa. This rapid increase highlights the trade-off between improved heat dissipation at higher velocities and the increased pumping power required to overcome the flow

resistance. The monotonic increase in pressure drop with coolant velocity follows a trend identical to that reported in a previous numerical study [14] on a Z-type configuration using cylindrical lithium-ion batteries.

4. Conclusions

In this study, we analysed a large-format prismatic lithium-ion battery pack with a Z-type cooling configuration. A commercial CFD tool employing the finite element method was used to solve the governing equations of heat transfer and fluid flow. A Z-type configuration, containing 4 cells, each arranged with a uniform inter-cell spacing in 2 rows was investigated across different geometric and operating conditions. We made use of the lumped battery, laminar flow, and heat transfer in solids and fluids physics interfaces in conjunction with multiphysics coupling features such as electrochemical heating and non-isothermal flow to carry out the numerical simulation. The solver was validated with the experimental data corresponding to a large-format prismatic cell with a rated-capacity of 157 Ah under 1C rate. Two parametric sensitivity studies were then performed to quantify the effects of (i) inter-cell spacing (3 mm to 10 mm) and (ii) coolant velocity (0.25 m/s to 1.5 m/s) on temperature uniformity and heat dissipation within the battery pack.

The simulation results indicate that the coolant velocity has a greater influence on the heat dissipation than the inter-cell spacing. As the coolant velocity increases from 0.25 m/s to 1.5 m/s, the average cell temperature drops from 310.84 K to 307.85 K. The present simulations show an inverse-relationship between the cell temperature and coolant velocity for the Z-type cooling configuration investigated in this study. Though the observed pressure drop across the different range of velocities studied fall within the desired limit, the results highlight the trade-off between enhanced heat dissipation and increased flow resistance. Furthermore, under the forced convection operation, increasing the inter-cell spacing from 3 mm to 10 mm led to a reduction in the pack-average cell temperature difference by 1.02 K, while the reduction in the maximum cell temperature difference is about 0.88 K. However, increasing the inter-cell spacing beyond 6 mm yields only slight improvement in the heat dissipation, and it is also important to have a balance between the energy density and thermal stability. The analysis conducted under natural convection conditions demonstrates that increasing the inter-cell spacing becomes less attractive due to stagnant air and thermal stratification. There is also a noticeable higher temperature in the central cells at the upstream and the downstream sections of the pack due to the thermal shielding effect. For the Z-type cooling configuration studied, an inter-cell spacing of 5 mm and a coolant velocity of 1.5 m/s appear to provide a suitable trade-off between effective heat dissipation and pressure drop across the range of conditions considered.

Acknowledgments

The research presented in this paper was developed within the project “Best4Grid – Vehicle battery storage for green transport and grid stability in the Nordics”, which is part of the Nordic Grand Solutions Programme funded by Nordic Energy Research. The financial support is gratefully acknowledged.

Nomenclature

C_p	specific heat at constant pressure, J/(kg K)
CS	inter-cell spacing, mm
$CC-CV$	constant current-constant voltage
$\frac{D()}{Dt}$	material derivate, s^{-1}
E	electrochemical potential, V
$\vec{g}$	gravitational acceleration, m/s
I	current, A
k	thermal conductivity, W/(m K)
p	pressure, Pa
Q	cell capacity, Ah
q	heat generation, W/m^3
SOC	state of charge
t	time, s
T	temperature, K
$\vec{V}$	velocity vector, m/s

Greek symbols

ρ	density, kg/m^3
μ	dynamic viscosity, Pa.s
β	isobaric coefficient of thermal expansion, K^{-1}

η_{IR}	ohmic voltage loss, V

Subscripts

1C	one-hour charge or discharge rate
amb	ambient
$\hat{n}$	unit-normal vector
o	initial/reference
ocp	open-circuit potential
ref	reference state

References

[1] Bashir Z., Hussain R., Khoharo H., Jaffri J.A., Saroj A.L., Bashir S., Selvaraj J., Ahmad M.S., Next-generation thermal management systems for lithium-ion batteries: enhancing the performance and safety in electric vehicles. Journal of Environmental Chemical Engineering 2026; 14(3):122529.

[2] Al-Hanahi B., Ahmad I., Habibi D., Masoum M.A., Smart charging strategies for heavy electric vehicles. eTransportation 2022; 13:100182.

[3] Nykvist B., Olsson O., The feasibility of heavy battery electric trucks. Joule 2021; 5(4):901-13.

[4] Swift A., Porter J.M., Newman A.M., Economic implications of battery longevity in heavy-duty vehicles. Journal of Power Sources 2025; 660:238398.

[5] Soliman A.S., Cheng P., A comprehensive review of battery thermal management systems: Enhancing performance, thermal models, and economic analysis. Journal of Energy Storage 2026;153:120880.

[6] Fekri Y., Heyhat M.M., Salehzadeh F.J., Wang Z., Rahbari A. A review of thermal management systems for extreme fast charging Li-ion batteries. Applied Thermal Engineering 2025; 279(Part E):127870.

[7] Olabi A.G., Maghrabie H.M., Adhari O.H., Sayed E.T., Yousef B.A., Salameh T., Kamil M., Abdelkareem M.A. Battery thermal management systems: Recent progress and challenges. International Journal of Thermofluids 2022; 15:100171.

[8] Wankhede S., Pingale A.D., Kale A., Experimental investigation on thermal management of lithium-ion battery pack for formula student electric vehicle using air-cooling system. Energy Storage and Saving 2025;4(1):38-47.

[9] Hemavathi S., Kumar A.A., AkashKumar R., Kumar J.V., Advancements in thermal management and safety of Li-ion batteries for electric vehicles: Addressing thermal runaway and fire risk mitigation. Thermal Science and Engineering Progress 2026; 71:104561.

[10] De Santis M., Giusti I., Poli F., Piancastelli L., Liverani A., Design and production trade-offs in lithium-ion batteries from cell formats to electric vehicles. Cell Reports Physical Science 2026; 7(3):103162.

[11] Akbarzadeh M., Kalogiannis T., Jaguemont J., Jin L., Behi H., Karimi D., Beheshti H., Van Mierlo J., Berecibar M., A comparative study between air cooling and liquid cooling thermal management systems for a high-energy lithium-ion battery module. Applied Thermal Engineering 2021;198:117503.

[12] Argade S., De A., Optimization study of a Z-type airflow cooling system of a lithium-ion battery pack. Physics of Fluids 2024; 36(6):067119.

[13] Shi H., Liu M., Xu W., Zhu X., Zou Y., Yang K., Optimization on thermal management of lithium-ion batteries using computational fluid dynamics and air-cooling methods. International Journal of Electrochemical Science 2022;17(5):220550.

[14] Zhang S.B., He X., Long N.C., Shen Y.J., Gao Q., Improving the air-cooling performance for lithium-ion battery packs by changing the air flow pattern. Applied Thermal Engineering 2023; 221:119825.

[15] Afzal A., Samee A.M., Razak R.A., Ramis M.K., Effect of spacing on thermal performance characteristics of Li-ion battery cells. Journal of Thermal Analysis and Calorimetry 2019; 135(3):1797-812.

[16] Gocmen S, Gungor S, Cetkin E., Thermal management of electric vehicle battery cells with homogeneous coolant and temperature distribution. Journal of Applied Physics 2020; 127(23):234902 (1-12).

[17] Koorata P.K., Chandrasekaran N., Numerical investigation of cooling performance of a novel air-cooled thermal management system for cylindrical Li-ion battery module. Applied Thermal Engineering 2021; 193:116961.

[18] Liaw B.Y., Roth E.P., Jungst R.G., Nagasubramanian G., Case H.L., Doughty D.H., Correlation of Arrhenius behaviors in power and capacity fades with cell impedance and heat generation in cylindrical lithium-ion cells. Journal of Power Sources. 2003; 119:874-86.

[19] Bernardi D., Pawlikowski E., Newman J., A general energy balance for battery systems. Journal of the Electrochemical Society 1985; 132(1):5-12.